*ChemCatChem*

ChemCatChem
Chemistry Europe
European Chemical Societies Publishing

RESEARCH ARTICLE OPEN ACCESS

# Catalytic Transfer Hydrogenation Reactions of Glycerol Over Zr-Incorporated Zeolite Beta Prepared by a Mechanochemical Approach

Auguste Fernandes[1] | M. Filipa Ribeiro[1] | João P. Lourenço[1,2]

[1]Centro de Química Estrutural, Instituto Superior Técnico, Institute of Molecular Sciences, Universidade de Lisboa, Lisboa, Portugal | [2]Faculdade de Ciências e Tecnologia, Universidade do Algarve, Faro, Portugal

**Correspondence:** Auguste Fernandes (auguste.fernandes@tecnico.ulisboa.pt) | João P. Lourenço (jlouren@ualg.pt)

**Received:** 3 February 2026 | **Revised:** 28 March 2026 | **Accepted:** 22 April 2026

**Keywords:** glycerol | heterogeneous catalysis | mechanochemistry | renewable resources | zeolites

## ABSTRACT

Zr-containing zeolite beta catalysts were prepared by a post-synthesis procedure involving a dealumination followed by a mechanochemical step and tested in the gas-phase conversion of glycerol. The catalytic data indicate that the catalysts are active in the conversion of glycerol, promoting not only the typical dehydration but also its hydrogenolysis without an external source of hydrogen, resulting in the production of significant amounts of ethylene glycol and methanol. Partially framework-attached $(Si{-}O)_2Zr{=}O$ species were identified and are suggested to play an important role in the catalytic behavior of these materials.

## 1 | Introduction

The transition toward sustainable energy and chemicals production is crucial for mitigating climate change and reducing our reliance on fossil fuels. The chemical industry is a significant contributor to global greenhouse gas emissions, primarily due to its reliance on fossil fuels for both energy and raw materials. By substituting fossil-based feedstocks with renewable ones, the industry can significantly reduce its carbon footprint [1].

Glycerol is obtained in large quantities as a byproduct in the biodiesel industry. Biodiesel is an example of a sustainable fuel already in use in transportation, and due to the constraints imposed by climate change, its production is expected to increase in the future [2, 3], with the consequent increase in glycerol production. Although glycerol is used in various industries (cosmetics and pharmaceuticals, food additives, and coatings), its large production has already led to a surplus that will tend to increase, with the consequent reduction in the market price [4].

The utilization of glycerol by the chemical industry through the conversion to versatile feedstocks would not only help in reducing greenhouse gas emissions but also promote the concept of a circular economy [5, 6]. By converting a byproduct into valuable chemicals, the overall efficiency of biodiesel production is enhanced, waste is minimized, and the dependency on fossil feedstocks is reduced.

Due to its chemical functionalities and reactivity, the glycerol molecule can be converted, using suitable catalytic systems, into a wide variety of compounds of industrial interest, such as acrolein, acetol, lactic acid, acrylic acid, syngas, propanediols, or glycerol carbonate [5–7]. Zeolites have structural and chemical characteristics that make them particularly suitable for use as catalysts and/or catalyst supports for the conversion of glycerol. Several studies have demonstrated the ability of HZSM-5 or

HBEA zeolites [8–10] to promote the gas-phase dehydration of glycerol into acrolein and acetol. However, obtaining some glycerol-derived products requires bifunctional catalysis since they are obtained through cascade reactions involving acid and redox-active centers. Examples of these products are allyl alcohol, acrylic acid, 1,2-propanediol, 1,3-propanediol, or lactic acid, for which zeolites have already been successfully studied. The tunable acidity of the zeolites can be combined with a redox function obtained by supporting a metal compound on their surface, as is the case of V/BEA and Fe/SZM-5 for the synthesis of allyl alcohol [11, 12], V/BEA for the synthesis of acrylic acid [13], Ir/ReHUSY for 1-propanol [14], Cu/Y and Ir-$ReO_x$ZSM-5 for propanediols [15, 16], or Pt/Sn-MFI and Au-Pt@SnBEA for the direct synthesis of lactic acid or methyl lactate [17, 18]. For specific metals and zeolite structures, it is also possible to incorporate the metal into the zeolite framework, either occupying fully tetrahedral positions when the metal ion allows it, as is the case of Ti in the MFI structure [19], or using four coordination positions provided by the framework and completing its higher coordination with hydroxyl groups or other types of ligands, as reported, for example, for W-ZSM-5 [20]. The framework incorporation is often incomplete, and less than four metal-framework oxygen bonds are formed, being the remaining coordination position occupied by an OH group ("open" metal site) along with the consequent appearance of a framework silanol [21, 22].

The metal incorporation can be achieved during the hydrothermal synthesis of the zeolite or by post-synthesis modifications. The incorporation by direct hydrothermal synthesis usually requires the use of toxic $F^-$ as a mineralizing agent, since the metal tends to form insoluble hydroxides under highly alkaline conditions usually used during zeolite synthesis, or, alternatively, requires complex synthesis procedures [21]. In the case of zeolite beta, post-synthesis dealumination-metalation strategies are very promising, since they involve short periods of time and allow better control of the metal content. The solid–gas reaction at moderate/high temperature involving the dealuminated zeolite and gaseous $SnCl_4$ was reported as an effective way of incorporating Sn [23]. However, it has also been shown to give rise to the formation of extra-framework $SnO_2$ [23]. An alternative solid-state ion exchange (SSIE) method consists in introducing the metal by using a mechanochemical-assisted synthesis approach where metal precursor and dealuminated zeolite are ground together for a specific period of time before calcination [21, 24]. This SSIE method is time-saving and limits the use of solvent and the subsequent waste production. It also proved to be adequate for other metals, such as Zr and Hf [21]. Sn- and Zr-incorporated zeolites are of particular interest because these metals enhance the Lewis acidity of the parent structure, a key feature for many catalytic processes [21, 25–28]. However, despite their potential, Zr-based zeolites remain far less studied than their Sn-based analogues.

Some examples are known where Zr-containing mesoporous silica or zeolites are active in the conversion of glycerol. C. García-Sancho et al. [29] prepared various samples of Zr-MCM-41 and tested them in the gas-phase dehydration of glycerol under conditions comparable to the ones used in this work. The results indicated that the main reaction products were acetaldehyde, acrolein, and acetol, as expected from an acid catalyst. On the other hand, A. Kant et al. [30] investigated a Zr-supported H-beta zeolite, prepared by wet impregnation, in the hydrogenolysis of glycerol in a batch reactor under hydrogen. The authors found out that the acidity of the zeolite plays a significant role in the final products' distribution, where, for both H-beta and Zr/H-beta, the main product was 1-propanol, followed by 1,2-propanediol as the second most abundant product.

In this work, we intend to explore the catalytic activity of framework-incorporated Zr-beta zeolite in the gas-phase conversion of glycerol without external hydrogen. In these conditions, two common products typically obtained over acid catalysts are acrolein and acetol. The reaction pathways leading to these products, which involve dehydration reactions, are strongly dependent on the acidity (i.e., number, nature, and strength of acid sites) [31–33]. However, the presence of a metal can also promote other reactions, such as hydrogen transfer, enabling the formation of different compounds [32].

Although the main objective of incorporating Zr into the beta zeolite framework was to generate Lewis acidity, the results demonstrate that this material is capable of promoting reactions beyond simple dehydration. This broadens the catalytic versatility of Zr-incorporated beta zeolite and highlights its potential for upgrading glycerol into value-added platform chemicals.

## 2 | Results and Discussion

### 2.1 | Preparation and Characterization of the Catalysts

In this study, a commercial beta zeolite with a Si/Al ratio of 12.5 was dealuminated using nitric acid and subsequently employed as a base material for supporting and/or incorporating zirconium (Zr) species through a mild, solvent-free mechanochemical SSIE grinding process. The method is easy to implement, does not require any solvent, and, above all, does not make use of a corrosive and toxic $F^-$ mineralizing agent. Because the formation of extra-framework Zr species may be influenced by subsequent washing steps, multiple samples were prepared to investigate how both framework-incorporated and extra-framework Zr species affect the catalytic performance in glycerol conversion. For comparison purposes, the same procedure was applied to a support in which framework incorporation of Zr is not likely to happen. SBA-15 was selected for this role, and after calcination, it yielded a material containing only Zr oxide dispersed onto the silica surface. This sample serves as a reference for Zr oxide to distinguish the catalytic contributions of framework-incorporated Zr species. Additionally, the catalytic behavior of the parent dealuminated beta zeolite was evaluated to establish a baseline, enabling a clearer assessment of the specific contribution of the zirconium species.

Table 1 displays the amount of Zr in the various samples. The parent dealuminated zeolite (BEA deal) used for the preparation of the other samples has a Si/Al ratio above 1000, which indicates that nearly all the Al atoms were removed from the framework. In the case of ZrBEA sample, it is clear that the washing step with methanol removes a substantial amount of metal, as described by Pornsetmetakul et al. [21], which in turn explains the PXRD results of this sample: methanol probably removes the non-

**TABLE 1** | Amount of Zr and textural parameters of the Zr-containing samples prepared.

| Sample | Zr wt.% | Si/Zr[a] | Mic. vol. ($cm^3.g^{-1}$)[b] |
|---|---|---|---|
| ZrBEA | 2.95 | 40.6 | 0.145 |
| ZrBEA-NW | 9.28 | 15 | 0.136 |
| ZrSBA-NW | 9.28 | 15 | n.d. |

[a]Molar ratio, considering the total framework-incorporated and extra-framework Zr in the sample.

[b]Determined by *t*-plot method. For the parent HBEA, the value is 0.172 $cm^3.g^{-1}$.

framework-bonded metal, and, consequently, no oxide phase is observed (see next).

The micropore volumes, presented in Table 1, indicate that the increase in the amount of Zr in the sample ZrBEA-NW did not have a significant impact on the porosity of the zeolite. The micropores' volume decreased by only 6% when compared with the sample ZrBEA. Therefore, no significant differences in mass diffusion constraints due to porosity are expected in these two samples.

The post-synthesis incorporation of Zr into the zeolite beta framework implies a prior dealumination of the structure, ensuring that it maintains its integrity. The PXRD patterns of the various samples prepared, shown in Figure 1, indicate that all the BEA-based samples maintain the typical pattern of the BEA zeolite. The sample that was not submitted to the washing procedure with methanol after the grinding step (ZrBEA-NW) shows, along with the pattern of BEA structure, diffraction peaks corresponding to monoclinic and tetragonal $ZrO_2$ phases (PDF 37-1484 and PDF 14-0534, respectively). The sample ZrSBA-NW only presents, as expected, the peaks corresponding to both $ZrO_2$ phases in the 2$\theta$ range analyzed. For sample ZrBEA, the results show that none of the $ZrO_2$ phases are present or, at least, the particles are too small to be identified by PXRD. The main peak of BEA zeolite at ca. 22.5° in 2$\theta$ has been shown to reflect structural changes in the zeolite lattice when Al atoms are removed or replaced by different heteroatoms [21, 28, 34]. The results found here (see inset in Figure 1) show, as expected, a contraction of the crystal lattice after the dealumination procedure (the peak is shifted to higher 2$\theta$ angles). However, in the case of the ZrBEA sample, no noticeable expansion is observed. This suggests that the amount of Zr occupying tetrahedral positions in the zeolite structure is not high enough to cause visible changes in the PXRD pattern. On the other hand, the sample ZrBEA-NW (having a much higher amount of Zr, as indicated in Table 1) evidences an expansion of the crystal lattice when compared with the dealuminated sample and, therefore, a higher amount of Zr in tetrahedral positions.

UV–vis spectroscopy has been largely used to obtain information about the local environment of metals in solid matrices. For Zr, it is well established that the presence of tetrahedral-coordinated Zr gives rise to an adsorption band in the 205–215 nm range attributed to a charge-transfer transition of an oxygen atom to an isolated Zr cation. In contrast, extra-framework $ZrO_2$ clusters can be identified by a band at about 230 nm [35–37]. Additionally, a broad band at around 260 nm is indicative of $(Si{-}O)_2{-}Zr{=}O$ species, corresponding to open Zr sites [37, 38].

Figure 2 displays the UV–vis spectra, in the region 200–350 nm, for all the samples prepared. The spectra recorded using Spectralon as a reference (Figure 2A) show, for all the samples, a broad band in the range 212–222 nm. Additionally, the samples ZrBEA-NW and ZrSBA-NW show a shoulder at around 230 nm. Regarding this shoulder, the spectrum of a commercial sample of $ZrO_2$ (Aldrich) (Figure 2A-e) confirms that it is due to the presence of extra-framework $ZrO_2$. Since this band does not appear in the spectrum of the sample ZrBEA, this sample is probably free of these $ZrO_2$ species, as already indicated by PXRD.

To confirm whether the higher energy band could have any contribution normally associated with the presence of tetrahedral Zr, we recorded new UV-vis spectra of the Zr-containing BEA, using the dealuminated BEA sample as a baseline. The results are shown in Figure 2B and indicate that the sample ZrBEA-NW has indeed tetrahedral Zr incorporated in the Al vacant sites (band at wavelength lower than 220 nm). Regarding the ZrBEA sample, although the presence of tetrahedrally coordinated Zr cannot be discarded (as suggested by the increased intensity below 220 nm), it seems that the major part of the Zr is present as $(Si{-}O)_2{-}Zr{=}O$ species, evidenced by the broad band at

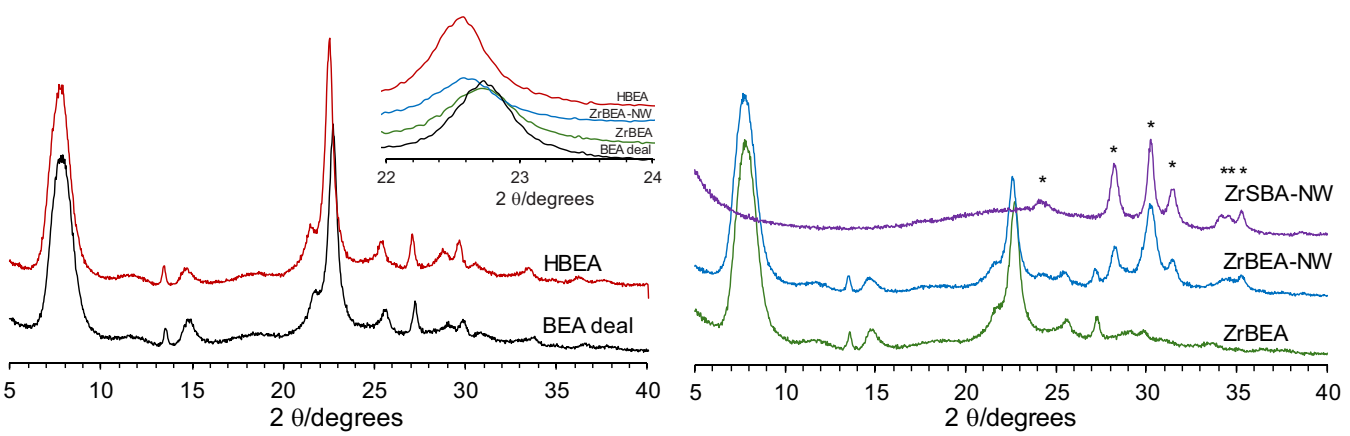


**FIGURE 1** | Powder XRD patterns of the various samples prepared. (*) denotes peaks from $ZrO_2$ (see the text for more details).

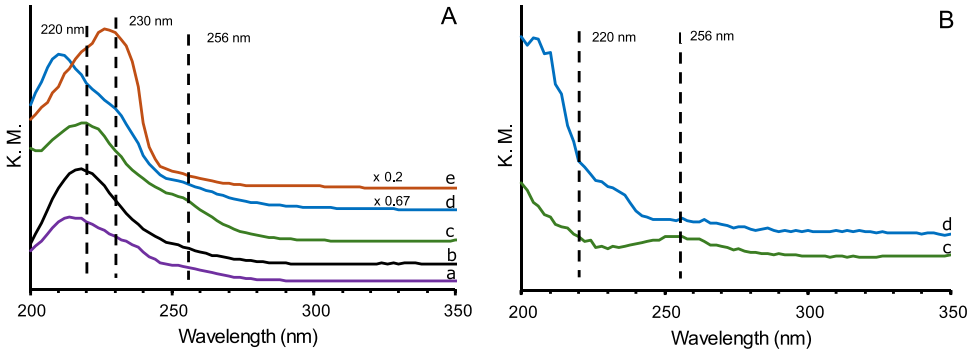


**FIGURE 2** | UV–vis. spectra of the different samples prepared (A) and UV–vis. spectra recorded with dealuminated BEA sample as baseline (B): (a) ZrSBA-NW, (b) BEA deal, (c) ZrBEA, (d) ZrBEA-NW, and (e) commercial $ZrO_2$.

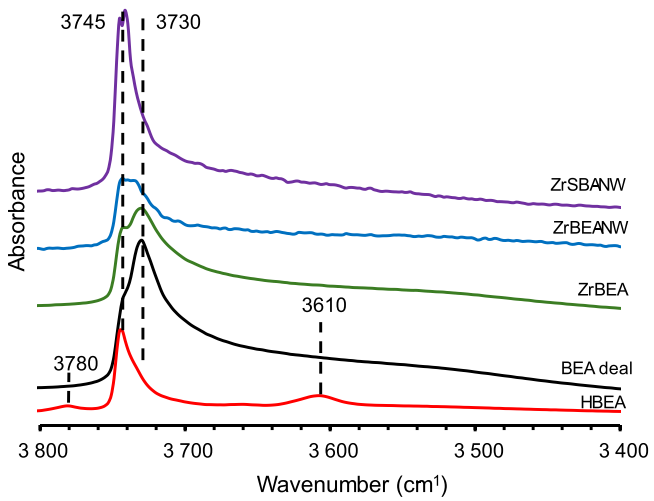


**FIGURE 3** | FTIR spectra of the different samples in the hydroxyl region (3800–3400 $cm^{-1}$).

256 nm. In the non-washed sample, this band is less pronounced, suggesting a lower concentration of these species, although ZrBEA-NW contains a significantly higher overall Zr content.

Dealumination of the BEA zeolite parent material leads to the formation of additional hydroxyl nests, which are expected to react with the metal species to be incorporated. This process can be monitored by assessing the changes in both the amount and the nature of the hydroxyl groups within the zeolite structure. Figure 3 displays the FTIR normalized (same wafer mass) spectra in the hydroxyl region (3800–3400 $cm^{-1}$) for the various samples. The parent HBEA zeolite shows the typical IR bands at 3780, 3745, and 3610 $cm^{-1}$, assigned respectively to Al—OH groups, external terminal Si—OH, and bridging acidic hydroxyls Si—Al—(OH)—Si. Upon the dealumination procedure, a new intense band at 3730 $cm^{-1}$, assigned to isolated internal Si—OH groups, and a broad band at ca. 3550 $cm^{-1}$ due to H-bonded silanol groups are clearly visible, along with the vanishing of the bands at 3780 and 3610 $cm^{-1}$. The disappearance of the bands associated with the bridged hydroxyl groups connected to framework Al atoms and the appearance/enhancement of bands assigned to internal silanol groups and H-bonded silanols indicate the formation of structure defects associated with silanols (silanol nests) upon aluminum removal [39]. The spectra of the samples ZrBEA and ZrBEA-NW show a significant decrease in the intensity of the band at 3730 $cm^{-1}$ observed for the dealuminated zeolite (BEA deal). This reduction can be attributed to the incorporation of $Zr^{4+}$ ions into the defects created by the Al (III) removal. No peaks associated with bridging hydroxyls were observed, as none were expected to appear since the introduction of Zr(IV) species does not create framework charge-balancing sites. In the case of the sample ZrBEA-NW, the band assigned to the terminal silanols was also perturbed, probably due to the deposition of large clusters of $ZrO_2$ (consistent with its higher Zr content compared to the ZrBEA sample). This phenomenon appears to result in a broader distribution of bond energies for both types of silanols, leading to less resolved bands. The spectrum of ZrSBA-NW further highlights the weak interaction between Zr species and the surface silanols of SBA-15, as the intensity of the isolated Si-OH groups remains essentially unchanged relative to that of the SBA-15 support.

**TABLE 2** | Acid properties of the various samples.

| | Acid sites (μmol.$g^{-1}$) | | | |
|---|---|---|---|---|
| | Lewis | | Brönsted | |
| Sample | 150°C | 300°C | 150°C | 300°C |
| HBEA | 355 | 295 | 553 | 271 |
| BEA deal | 5 | 2 | 0 | 0 |
| ZrBEA | 93 | 12 | 38 | 12 |
| ZrBEA-NW | 98 | 7 | 10 | 0 |
| ZrSBA-NW | 12 | 0 | 0 | 0 |

The acidity of the catalysts is of primary importance in the conversion of glycerol, since the main reaction pathways, such as those involving dehydration and hydrogenolysis, depend on the number and nature of the acid sites [29, 40]. Pyridine (Py) adsorption was used to distinguish between Brönsted and Lewis acid sites and to quantitatively evaluate their concentration in the various prepared samples. The number of acid sites measured for each sample is presented in Table 2.

As expected, dealumination of the parent zeolite resulted in a pronounced decrease in the acidity. The mechanochemical procedure followed by the thermal treatment, aiming to incorporate

Zr into the zeolite framework, resulted in the generation of both Lewis and Brönsted acid sites, with the major proportion being Lewis acid sites. Table 2 also shows that the most important fraction of the acid sites is essentially weak, since most of the Py is desorbed at 300°C.

In the case of an aluminosilicate framework, the presence of linked $AlO_4$ and $SiO_4$ tetrahedra creates a local charge imbalance, which is recognized as the main reason for the existence of Brönsted acid sites when the compensation cation is a proton. Considering that Zr(IV) occupies the T-vacant sites generated by the removal of aluminum ($Al^{3+}$), either as tetrahedrally coordinated Zr or as $(Si{-}O)_2{-}Zr{=}O$ species, no formal framework local charge imbalance exists. Therefore, the presence of Brönsted acidity cannot be explained in this case by the same mechanism. Garcia-Sancho et al. and P. Salas et al. [29, 41] explained the appearance of Brönsted acid sites in Zr-incorporated MCM-41 material prepared by hydrothermal synthesis by proposing that the substitution of a Si(IV) ion with a larger Zr (IV) ion in the silica framework induces structural microstrain and changes the electronic density around neighboring Si atoms. The substitution of a Si atom in the vicinity of a Si—OH group weakens the hydroxyl bond and generates Brönsted acidity. Assuming that a similar process occurs in the case of Zr-containing BEA samples prepared in this study, the presence of Brönsted acid sites can be attributed to a fraction of Zr (IV) species incorporated into the BEA framework. In contrast, for the ZrSBA-15 sample, which was prepared by a post-synthesis procedure, substitution of Si by Zr is not expected to occur, thereby explaining the absence of significant acidity.

When comparing the acidity with the final Zr content of ZrBEA and ZrBEA-NW samples, it is clear that only part of the $ZrCl_4$ used in the grinding process was effectively incorporated into the zeolite structure and contributed to generate acidity. The number of Lewis acid sites is similar in both samples, while the number of Brönsted acid sites is slightly lower in the ZrBEA-NW sample, which also has fewer strong acid centers. These results suggest that the formation of $(Si{-}O)_2{-}Zr{=}O$ species, more evident in the ZrBEA sample despite its lower Zr content, may play a key role in the development of acidity, as no differences in the Py accessibility are expected. The methanol washing procedure not only removes the excess of $ZrCl_4$ but probably also enhances the dispersion of Zr species, leading to increased incorporation during the subsequent thermal treatment. In summary, mechanochemical-assisted solid-state ion exchange, followed by methanol washing, seems to be a very impacting synthesis method to obtain highly dispersed and isolated Zr species with very distinct chemical properties.

## 2.2 | Catalytic Tests

The modification of zeolites with Zr has been commonly carried out to prepare Lewis acid catalysts [21, 42, 43]. Indeed, the results of Py adsorption confirm that the amount of Lewis acid sites that are generated by Zr incorporation is greater than that of Brönsted acid sites. In this context, the samples were then tested as catalysts for the gas-phase conversion of glycerol, a reaction known to be highly sensitive to the nature of the catalyst's acid sites.

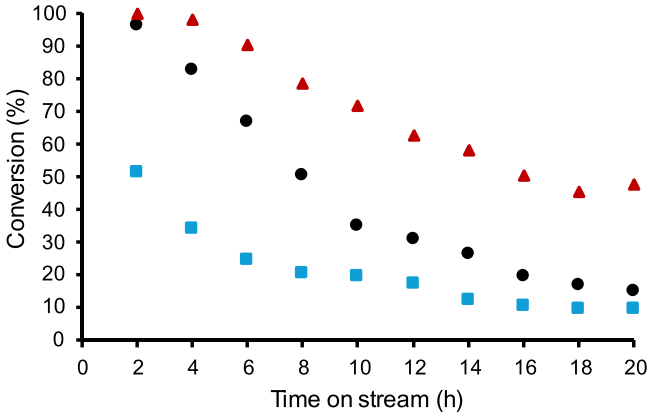


**FIGURE 4** | Conversion of glycerol over ZrBEA: (■) 280°C, (●) 300°C, and (▲) 330°C.

Figure 4, which presents the evolution of the conversion of glycerol at different temperatures as a function of the time on stream, shows that ZrBEA sample is an active catalyst for this reaction. At a reaction temperature of 280°C, the initial conversion was 52%, but rapidly decreased, reaching 10% after 20 h on stream. Increasing the temperature to 300°C, the conversion increases considerably but again gradually decreases to reach 15% after 20 h on stream. The catalyst was also tested at 330°C, and the results show complete glycerol conversion during the first 2 h of reaction, which decreased to 48% after 20 h on stream.

Deactivation of acid catalysts in gas-phase reactions is usually associated with the formation and deposition of coke. However, taking into consideration that in this case the acidity of the catalysts is rather low, we must also consider the high polar nature of both reactants and products, which will constrain the molecules' diffusion. When the temperature increased from 280°C to 330°C, no significant changes were observed regarding the amount of coke formed (Table 3), and, therefore, in these conditions, the decrease of mass transfer constraints should be the main factor affecting the deactivation. Due to the high polarity of reagents and products, an increase in temperature avoids excessive adsorption by the zeolite surface and facilitates the circulation of the main compounds. The lower deactivation rate verified at 330°C seems to agree with this interpretation.

The products' selectivity for representative values of time on stream (2 and 10 h) are presented in Table 3. The graphics showing the selectivity toward the various products for the complete time on stream are presented in Figure S1. Data in this table show the formation of acrolein and acetol, which are typical reaction products from the dehydration of glycerol over acid catalysts [2, 3, 8–10], but also compounds that are not usual to be found in significant amounts among the reaction products obtained in these conditions, namely, methanol, 1,2-propanediol and ethylene glycol. It should be noted that other identified (such as propanal, acetone, ethanol, allyl alcohol, acetic acid, 1,3-dioxan,5-ol, and 2,3-butadione) and non-identified products were also present, but none exceeding 5% selectivity, and some were found only in trace amounts. 1-Propanol and 1,3-propanediol, two of the compounds often formed by hydrogenolysis, were not detected or were just detected in trace amounts. Carbon dioxide and carbon monoxide are probably also formed, but our catalytic

**TABLE 3** | Main reaction products obtained at different temperatures using ZrBEA as catalyst.

| | 280°C | | 300°C | | 330°C | |
|---|---|---|---|---|---|---|
| **Time on stream** | **2 h** | **10 h** | **2 h** | **10 h** | **2 h** | **10 h** |
| Conversion (%) | 52 | 20 | 97 | 35 | 100 | 72 |
| Selectivity (%) | | | | | | |
| Acetaldehyde | 6.2 | 4.8 | 9.2 | 7.1 | 11.5 | 9.8 |
| Acrolein | 13.9 | 16.9 | 6.4 | 12.9 | 6.0 | 16.9 |
| Methanol | 6.6 | 10.0 | 13.7 | 12.1 | 14.8 | 12.8 |
| Acetol | 14.9 | 23.1 | 13.5 | 20.4 | 8.7 | 14.1 |
| 1,2-propanediol | 6.7 | 8.4 | 2.5 | 5.3 | 0.7 | 3.2 |
| Ethylene glycol | 9.8 | 17.0 | 11.7 | 18.2 | 6.7 | 13.7 |
| $Sel_{eth\ glyc}/Sel_{methanol}$ | 1.48 | 1.70 | 0.85 | 1.50 | 0.45 | 1.07 |
| Carbon bal. (%)[a] | 67 | 88 | 59 | 78 | 56 | 71 |
| Coke (%)[b] | 15.2 | | 15.4 | | 15.1 | |

[a]Carbon balance includes all the products that were recovered and identified.
[b]Determined after time on stream of 20 h, as the weight loss in the range 100°C–700°C.

setup does not allow their quantification. The carbon balance shown in Table 3 reflects the fraction of carbon recovered in the identified products. As only the compounds listed in the table were considered in this calculation, the values are lower than 100%. The remaining carbon corresponds to identified products not included due to their occurrence in small or trace amounts, as well as non-identified compounds, CO and/or $CO_2$, and the coke deposited on the catalyst. The decrease of the carbon balance with the temperature reflects the increased formation of unrecovered gaseous products.

Hydrogenolysis of glycerol aiming at the production of propanediols has been a subject of intense study in the last years, mostly due to the industrial importance of these compounds [15, 16, 44]. As hydrogenolysis involves the addition of hydrogen to the fragments of a previous C—C or C-heteroatom bond dissociation, these reactions are usually carried out in liquid or gas phase under $H_2$ atmosphere. Nevertheless, hydrogenolysis of glycerol has also been shown to occur in the absence of external $H_2$, either by the consumption of a part of the glycerol (via steam reforming) or by the consumption of an H-donor added from external sources (alcohols, carboxylic acids) [44] or produced in situ (glycerol can also act as a hydrogen donor) [32]. In this work, no external $H_2$ or H-donors were used, and, therefore, the hydrogen needed for the hydrogenolysis reaction was provided by glycerol and/or reaction intermediates with OH functionalities.

A closer examination of the data presented in Table 3 reveals that the products' formation is strongly influenced by the reaction temperature. The formation of acetaldehyde tends to increase with temperature, probably because it is a final product. On the other hand, the selectivity to 1,2-propanediol and acetol suffers a decrease with the temperature, which might indicate that these products have undergone a subsequent transformation, which is more evident with the increase of the temperature.

The most surprising result found in this set of catalytic data is the formation of ethylene glycol and methanol in such significant amounts. Ethylene glycol is often mentioned in the literature as one of the products obtained in the hydrogenolysis of glycerol to propanediols [15, 45–49], but usually the reaction involves the use of external $H_2$ and sometimes expensive catalysts, such as Ru or Pt. In the present case, the catalyst not only allows the hydrogenolysis of glycerol without the addition of $H_2$ involving the C—O bond but also promotes the scission of a C—C bond, which is characteristic of Ru-based catalysts [50]. In a comprehensive review from S. Kandasamy et al. [51], the authors concluded that heterogeneous catalysis involving transition metals and noble metal catalysts can be an important route to the production of ethylene glycol via glycerol hydrogenolysis. Catalysts containing Cu, Ni, W, or Mo metals show good results for the conversion of glycerol via hydrogenolysis, while metals, such as Ru, Pt, Pd, or Ir enhance the selectivity toward ethylene glycol due to the ability to promote the dissociation of a C—C bond. Catalysts containing more than one metal are often used, taking advantage of the different metal behavior. An example is the work of N. Ueda et al. [52] that used Pt-modified $Ni/Al_2O_3$ catalysts in the liquid phase under 8.0 MPa $H_2$. The authors obtained ethylene glycol, 1,2-propanediol, and methane as main products (methanol was barely obtained) and concluded that Pt played an important role in the formation of ethylene glycol and methane by either promoting retro-aldol reaction of glyceraldehyde or the dissociation of a C—C bond.

Another example of hydrogenolysis of glycerol under a hydrogen atmosphere was reported by Kant et al. [30], who employed Zr supported in a H-beta zeolite prepared via conventional impregnation. Their results indicated that catalyst acidity was the primary factor governing catalytic performance, leading predominantly to the formation of 1-propanol and 1,2-propanediol. In the present work, the Zr catalyst was prepared using a different approach, in which the Zr was incorporated into the framework of zeolite beta, and the resulting acidity was generated as a result of this incorporation. To the best of our knowledge, this is the first report on the use of a Zr-incorporated zeolite with these characteristics for the conversion of glycerol. The results exhibited in Table 3 clearly show that this catalyst not only catalyzes the typical dehydration of glycerol but also promotes its hydrogenolysis, involving both C—O and C—C bond cleavage.

To evaluate whether the incorporation of zirconium into the zeolite framework is a primary determinant of the resulting product distribution, two comparative samples were examined: one containing both framework-incorporated and extra-framework zirconium species (ZrBEA-NW) and another containing exclusively extra-framework zirconium in the form of zirconium oxide dispersed on a silica surface (ZrSBA-NW). Their catalytic performance was compared with that of the ZrBEA sample.

Figure 5 displays the conversion of glycerol obtained with all the samples. The conversion obtained with ZrBEA is significantly higher than that obtained with the other Zr-containing samples, although this sample has less Zr (3 wt.% for ZrBEA and 9.3 wt.% for both ZrBEA-NW and ZrSBA-15). These results indicate that ZrO2 supported on either beta zeolite or SBA-15 (as confirmed

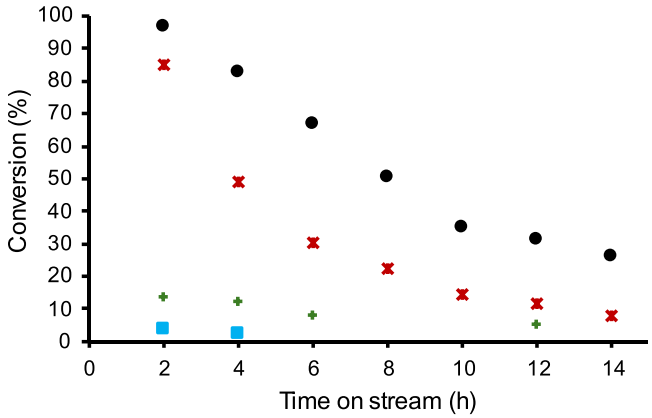


**FIGURE 5** | Conversion of glycerol at 300°C over ZrSBA-NW (■), BEA deal (+), ZrBEA-NW (✳), and ZrBEA (●) samples.

by XRD) is not significantly active for the conversion of glycerol under the conditions of this study. In fact, the ZrSBA-NW sample exhibits very low catalytic activity from the beginning of the reaction, with conversion values below 5%. The conversion exhibited by the BEA-deal sample, although somewhat higher than that obtained with ZrSBA-NW, remains significantly lower than that achieved with the Zr-containing BEA samples, as would be expected given its low acidity.

Figure 6 shows the selectivity to the main reaction products obtained with the samples ZrBEA and ZrBEA-NW. Regarding the sample ZrSBA, the low conversion makes difficult the accurate determination of the selectivity of each product, however, within these constraints, the results indicate that the main products obtained with this sample were acrolein and acetol, with a total selectivity of more than 60%. The dealuminated BEA sample exhibits a comparable catalytic profile, with acrolein, acetol, and acetaldehyde collectively accounting for more than 90% of the observed selectivity. No products associated with hydrogenolysis, such as propanediols, methanol, or ethylene glycol, were detected. For the other two samples, the products' distribution is rather similar, at least in the first hours on stream. These results, when combined with the characterization data, suggest that the active sites of these samples are mainly the framework-incorporated Zr atoms (closed and/or open Zr sites). As shown above, the sample ZrBEA-NW has a higher amount of Zr, but part of the metal is supported in the form of $ZrO_2$. The number of acid sites measured by Py adsorption is similar for both samples, indicating that the same amount of Zr was in fact incorporated. The results obtained with the sample ZrSBA-NW are in line with this conclusion, as no incorporation is expected to occur, and, therefore, in the conditions of this work, only a very low activity was observed, with the main reaction products being those resulting from dehydration (acrolein and acetol).

## 2.3 | Mechanistic Considerations

Hydrogenolysis of glycerol to 1,2-propanediol has been studied with a large variety of catalysts and reaction conditions. Regarding the reaction mechanism, three main mechanistic pathways have been proposed in the literature, depending on the nature of the catalyst and other experimental conditions [53]: (a) dehydrogenation–dehydration–hydrogenation (glyceraldehyde route), (b) dehydration-hydrogenation, and (c) direct glycerol hydrogenolysis (Scheme 1).

The first step in route (a) involves the hydrogenation of glycerol to glyceraldehyde over the metal catalyst, but the presence of a base is usually required to promote the dehydration of this intermediate and to prevent its subsequent hydrogenation back to glycerol. The hydrogenation of 2-hydroxyacrolein (or pyruvaldehyde obtained by keto-enol tautomerism) yields 1,2-propanediol [15, 54, 55] (Scheme 1a). It has been suggested that, under alkaline conditions, glyceraldehyde can undergo retro-aldol reactions that produce ethylene glycol and methanol after hydrogenation. However, given the alkalinity requirements of this pathway, it is not expected to be the main route with our catalytic system. Over acid catalysts, route (b) has been the preferred pathway used to explain the formation of propanols [15, 30, 46]. Here, 1,2-propanediol is formed via hydrogenation of acetol (Scheme 1b). The third route (route c) has been proposed to explain the hydrogenolysis of glycerol over $ReO_x$ and Ir-$MO_x$ catalysts and involves the adsorption of glycerol on $MO_x$ sites, forming an alkoxide, while hydrogen is activated on a metal site to form a hydride [53, 54].

Ethylene glycol and methanol appear as degradation products in various mechanistic paths. As mentioned above, these products may be formed via retro-aldolization of glyceraldehyde with a subsequent hydrogenation of glycolaldehyde and formaldehyde (Scheme 1a). However, Miyazwa et al. [47], working with Cu/C and an ion-exchange resin under $H_2$, concluded that ethylene glycol and methanol were formed directly via the degradation of glycerol. In a similar way, Musolino et al. [56] concluded that ethylene glycol and methanol could be formed directedly from glycerol. In that work, the authors used an autoclave under 5 bar of inert atmosphere, $PdO/Fe_2O_3$ as the catalyst, and alcohols as hydrogen donors. This direct pathway is expected to give rise to stoichiometric quantities of ethylene glycol and methanol, and thus a ratio in the carbon selectivity (ethylene glycol/methanol) of 2. In the present work, this ratio is always lower than 2 (Table 3), suggesting that methanol may be formed from compounds other than glycerol and/or that ethylene glycol undergoes degradation to methanol or other gaseous products. In fact, the results obtained from catalytic tests at different temperatures support this assumption, as lower ratios are always observed at the beginning of the reaction, when the catalyst is more active, and the ratio further decreases with increasing temperature.

To shed some light on the formation of these two products, we carried out exploratory tests using ethylene glycol, acetol, and 1,2-propanediol as reagents. For that purpose, a sample of ZrBEA and a 10% aqueous solution of each reagent were used (the main results are shown in Table S1). The results suggest that methanol formation predominantly occurs from ethylene glycol, in which it is the main product, whereas its production from acetol or 1,2-propanediol is negligible. On the other hand, ethylene glycol is also produced from 1,2-propanediol. Other compounds identified in these reactions were acetaldehyde, ethanol (when using ethylene glycol as a reagent), and acetone (when acetol or 1,2 propanediol was used). Small amounts of acetol and 1,2-propanediol were also obtained when using 1,2-propanediol and acetol, respectively. It should be noted that neither ethanol nor

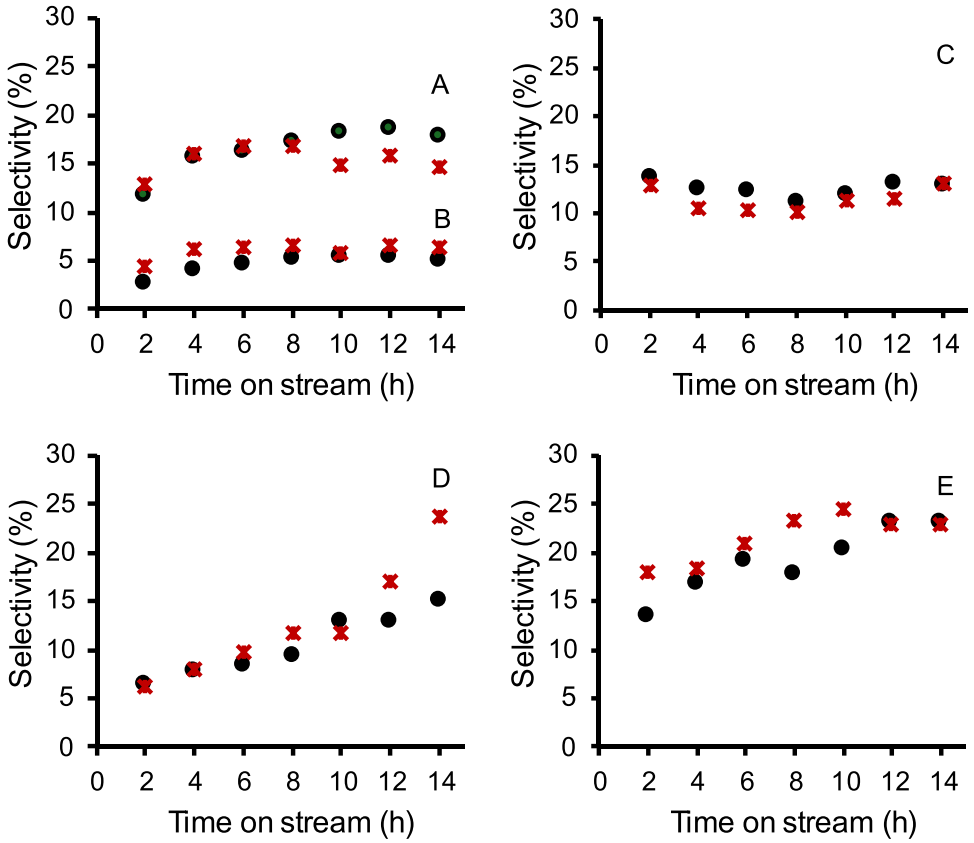


**FIGURE 6** | Selectivity to selected reaction products obtained with ZrBEA (●) and ZrBEA-NW (✳): (A) ethylene glycol, (B) 1,2-propanediol, (C) methanol, (D) acrolein, and (E) acetol.

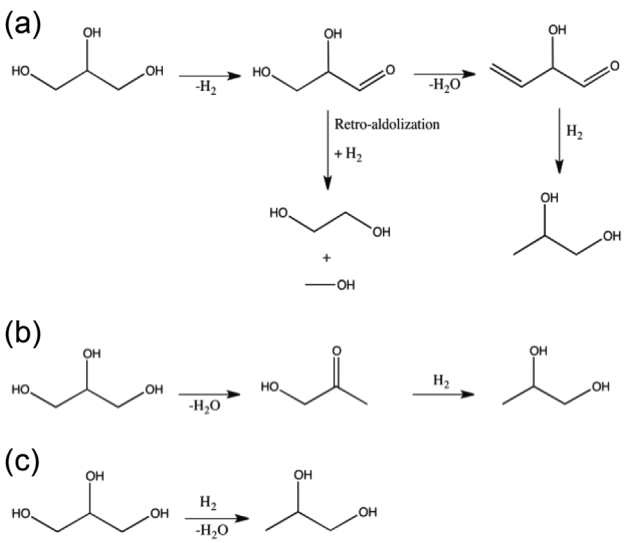


**SCHEME 1** | Simplified mechanistic pathways for the hydrogenolysis of glycerol to 1,2-propanediol.

acetone was obtained in significant amounts when the catalytic tests were carried out with glycerol, which may suggest that the degradation of the glycerol hydrogenolysis products (acetol, propanediol, and ethylene glycol) is not high enough to account for a major part of ethylene glycol and methanol produced. However, the lower ratios of ethylene glycol/methanol at higher temperatures and at the beginning of the reaction suggest that these degradation reactions (in particular, the formation of methanol at the expense of the ethylene glycol) could play a significant role in this catalytic system.

Acetaldehyde is another product of the reaction resulting from the degradation of several compounds. Tsukuda et al. [57] proposed that acetaldehyde could be formed from 3-hydroxypropanal, a precursor of acrolein in the dehydration of glycerol, via a retro-aldol reaction. On the other hand, several studies have reported that acetaldehyde can be formed through the cracking of acetol [58–60], and its presence has also been detected when using ethylene glycol and 1,2-propanediol as reagents. Considering these findings together with our own observations, we propose Scheme 2, which summarizes the reaction pathways that may account for the catalytic results obtained in this work.

## 2.4 | Regeneration of the Catalyst

Figure 7 compares the conversion achieved with a fresh ZrBEA sample to that obtained after four regeneration cycles (corresponding to five reaction runs). The data clearly demonstrates the high stability and good reusability of this catalyst. After these regeneration cycles, the catalyst recovers nearly all of its initial activity, and although a slight increase in the deactivation rate is observed, the activity after 20 h on stream remains very similar to that of the fresh sample. Regarding the selectivity to the main reaction products, there are no significant changes between

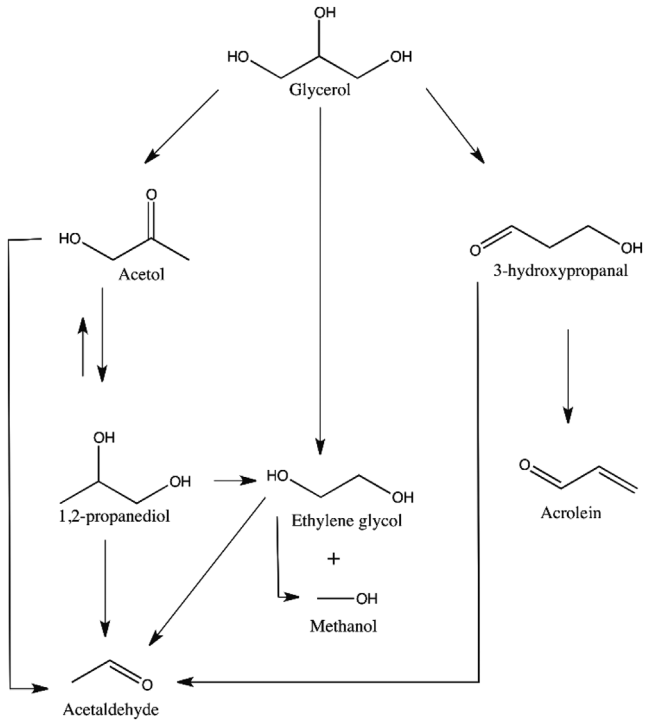


**SCHEME 2** | Schematic pathways for the formation of the main reaction products obtained with glycerol as a reagent.

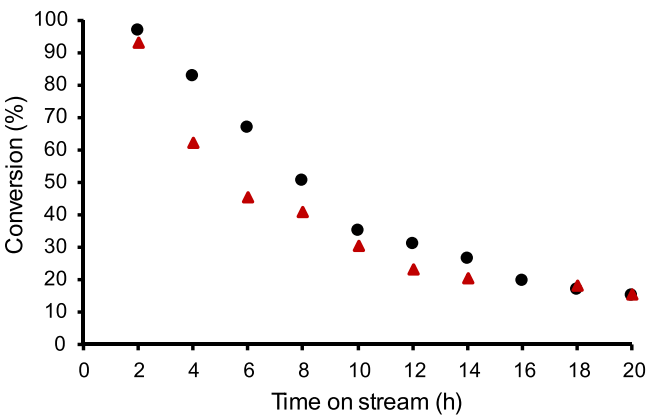


**FIGURE 7** | Conversion of glycerol over sample ZrBEA: (●) fresh sample and (▲) after four regenerations.

the first and the fifth cycle (see Figure S2), which reveals the stability of the active centers. Data on glycerol conversion for the first, second, and third regeneration cycles are shown in Supporting Information (Figure S3).

## 3 | Conclusion

This study demonstrates that incorporating Zr into the BEA zeolite structure via solid-state ion exchange using a mechanochemical procedure enables the preparation of catalysts that exhibit unusual behavior in the gas-phase conversion of glycerol. Indeed, combining mechanochemical-assisted ion exchange with methanol washing seems to be a strategy of choice to obtain Zr-based zeolite materials where metal is exclusively introduced as isolated framework species. Moreover, this simple grinding method offers an eco-friendly and low-cost alternative to more complex synthesis methods. On the other hand, although most reports on similar catalysts have focused on the formation of Lewis acid sites, this study demonstrates that the framework incorporation of Zr produces catalytic sites capable not only of promoting glycerol dehydration but also of catalyzing, to a significant extent, the hydrogenolysis of C—C and C—O bonds in the absence of external hydrogen, a behavior more commonly observed with Re-containing catalysts. The results suggest that the nature of the Zr environment plays a crucial role, with partially bonded species, such as $(Si—O)_2Zr═O$, being the most important in this process. Although further work is required to optimize the selectivity, these preliminary results, demonstrating the feasibility of producing ethylene glycol and methanol from glycerol, expand the potential of glycerol as a versatile platform chemical.

## 4 | Experimental Section

### 4.1 | Catalysts Preparation

The preparation of Zr-beta followed a two-step procedure adapted from that described by Pornsetmetakul et al. [21]. Commercial beta zeolite (Zeolyst CP814E, ammonium form, Si/Al ratio of 12.5) was dealuminated by treatment with a 12 M nitric acid solution at 80°C for 20 h, using a liquid to solid ratio of 10 mL $g^{-1}$. The dealuminated zeolite was washed with deionized water and dried in an oven at 100°C overnight. Tetravalent Zr was introduced by a mechanochemically-driven solid-state reaction. An appropriate amount of $ZrCl_4$ (corresponding to a Si/Me atomic ratio of 15) was ground in an agate mortar with the dealuminated zeolite for 15 min under ambient conditions. The mixture was then washed with 50 mL of methanol, dried in an oven at 60°C for 4 h, and finally calcined in a muffle furnace at 550°C for 6 h (sample ZrBEA). To evaluate the effect of framework metal incorporation and the presence of supported metal oxide, two additional samples were prepared without the methanol washing step: ZrBEA-NW and ZrSBA-NW (where NW means no washing). The SBA-15 material used as support was prepared according to the procedure described elsewhere [61]. In this case, the amount of $ZrCl_4$ used corresponds to that used for the preparation of ZrBEA samples (0.237 $g_{ZrCl4}/g_{SBA\text{-}15}$).

### 4.2 | Characterization

Bulk chemical analysis using AA and ICP-OES techniques was used to measure the amount of Si, Al, and Zr in the various samples. Powder x-ray diffraction (PXRD) patterns were recorded in a Bruker D8 Advance diffractometer with Cu $K_\alpha$ radiation filtered by Ni and a 1D LynxEye detector.

Py adsorption was followed by FTIR spectroscopy as described elsewhere [32]. Using a homemade glass cell, the sample was evacuated ($10^{-6}$ Torr) under heating (450°C, 2 h) and subsequently contacted with Py at 150°C (1.5 Torr). After outgassing the system for 30 min at 150°C, a spectrum was recorded. The temperature was then raised to 350°C, and after 30 min, a new spectrum was recorded. For both temperatures, the background spectrum, recorded under identical operating conditions but

without a sample, was recorded and automatically subtracted. For the quantitative measurement, integrated molar extinction coefficients determined in our experimental setup ($\varepsilon_B = 0.91$ cm.μmol$^{-1}$, Py adsorbed onto a Brønsted acid site, and $\varepsilon_L = 1.58$ cm.μmol$^{-1}$, Py adsorbed onto a Lewis acid site) were used. In order to compare the FTIR spectra of the various samples in the OH region (4000–3000 cm$^{-1}$), spectra were normalized to a mass of 20 mg.

DRS UV–vis spectra were obtained with a Praying Mantis accessory from Harrick coupled to a Thermo Scientific Evolution 300 spectrometer. The spectra were recorded using Spectralon as a standard in the range 200–800 nm.

The coke content was determined by means of thermogravimetric (TG-DSC) analysis. The TG-DSC data were obtained with Setsys Evo16 Setaram equipment, under air and with a heating rate of 10°C.min$^{-1}$ (temperature range 20°C–800°C).

Nitrogen sorption measurements at −196°C were performed on Autosorb IQ equipment (Quantachrome). Before nitrogen sorption, the samples were outgassed under vacuum at 90°C for 1 h and then at 350°C for 6 h. The *t*-plot method was used to determine the micropore volume.

### 4.3 | Catalytic Tests

Conversion of glycerol was carried out at different temperatures in the range of 280°C–330°C under atmospheric pressure in a fixed-bed borosilicate reactor (i.d. 1.5 cm) using 300 mg of catalyst. The reaction feed, an aqueous solution containing 20 wt.% of glycerol, was introduced in the reactor by a syringe pump KD Scientific at 2.5 mL.h$^{-1}$ and diluted in a flow of dry nitrogen (30 mL.min$^{-1}$). The liquid reaction products were collected in an ice trap, followed by two additional water traps. Reaction products recovered every 2 h were analyzed on an Agilent 6890N gas chromatograph equipped with a 30 m Ohio Valley OV351 capillary column and an FID detector. Selected samples were analyzed by GC-MS with a Shimadzu QP2020 NX and a 30 m Teknokroma FRB-FFAP capillary column.

The conversion of glycerol, the carbon selectivity, and the carbon balance were calculated as follows:

$$\%\ Conv = \frac{n_{g,total} - n_{g,t}}{n_{g,total}} \times 100$$

$$\%\ Sel_i\,(carbon) = \frac{n_{i,t}}{n_{g,total} - n_{g,t}} \times \frac{C_i}{C_g} \times 100$$

$$Carb.\ bal.\,(\%) = \frac{\sum CP_i}{Cconv} \times 100$$

where $n_{g,total}$ is the total number of moles of glycerol injected into the reactor during the time *t*, $n_{g,t}$ is the number of moles of glycerol recovered at time *t*, $n_{i,t}$ is the number of moles of the product *i* recovered at time t, $C_i$ is the number of carbon atoms in each molecule of product *i*, $C_g$ is the number of carbon atoms of glycerol (3), $CP_i$ is the carbon recovered of the product *i*, and $C_{conv}$ is the total carbon converted. For the determination of the carbon balance, only the products identified were considered. The analyses correspond to the products recovered for 2 h.

Reusability of the ZrBEA catalyst was assessed by regenerating the spent catalyst at 550°C for 5 h under a flux of dry air and carrying out a new catalytic test at 300°C.

#### Author Contributions

**João P. Lourenço**: conceptualization, investigation, writing – original draft, supervision. **M. Filipa Ribeiro**: conceptualization, funding acquisition, writing – review editing. **Auguste Fernandes**: investigation, writing – review editing, methodology.

#### Acknowledgments

The authors thank FCT for funding support UID/00100/2025, UID/PRR/100/2025 (CQE), and LA/P/0056/2020 (IMS). Auguste Fernandes also thanks FCT for FCT-Tenure program: contract 2023.15700.TENURE.029.

Open access publication funding provided by FCT (b-on).

#### Conflicts of Interest

The authors declare no conflicts of interest.

#### Data Availability Statement

The data that support the findings of this study are available from the corresponding author upon reasonable request.

#### References

1. A. Kätelhön, R. Meys, S. Deutz, S. Suh, and A. Bardow, "Climate Change Mitigation Potential of Carbon Capture and Utilization in the Chemical Industry," *Proceedings of the National Academy of Sciences of the United States of America* 166 (2019): 11187–11194.

2. F. F. Barbosa and T. P. Braga, "Catalytic Conversion of Glycerol to Acetol and Acrolein Using Metal Oxides: Surface Reactions, Prospects and Challenges," *ChemCatChem* 15 (2023): e202200950–e202200950.

3. A. Galadima and O. Muraza, "A Review on Glycerol Valorization to Acrolein Over Solid Acid Catalysts," *Journal of the Taiwan Institute of Chemical Engineers* 67 (2016): 29–44, https://doi.org/10.1016/j.jtice.2016.07.019.

4. Z. Pirzadi and F. Meshkani, "From Glycerol Production to Its Value-Added Uses: A Critical Review," *Fuel* 329 (2022): 125044–125044, https://doi.org/10.1016/j.fuel.2022.125044.

5. G. M. Lari, G. Pastore, M. Haus, et al., "Environmental and Economical Perspectives of a Glycerol Biorefinery," *Energy & Environmental Science* 11 (2018): 1012–1029, https://doi.org/10.1039/C7EE03116E.

6. M. N. Gatti, F. M. Perez, G. F. Santori, N. N. Nichio, and F. Pompeo, "Heterogeneous Catalysts for Glycerol Biorefineries: Hydrogenolysis to 1,2-Propylene Glycol," *Materials* 16 (2023): 3551, https://doi.org/10.3390/ma16093551.

7. S. Bagheri, N. M. Julkapli, and W. A. Yehye, "Catalytic Conversion of Biodiesel Derived Raw Glycerol to Value Added Products," *Renewable and Sustainable Energy Reviews* 41 (2015): 113–127, https://doi.org/10.1016/j.rser.2014.08.031.

8. Y. T. Kim, K. D. Jung, and E. D. Park, "A Comparative Study for Gas-Phase Dehydration of Glycerol Over H-Zeolites," *Applied Catalysis A: General* 393 (2011): 275–287, https://doi.org/10.1016/j.apcata.2010.12.007.

9. B. Katryniok, S. Paul, V. Bellière-Baca, P. Rey, and F. Dumeignil, "Glycerol Dehydration to Acrolein in the Context of New Uses of Glycerol," *Green Chemistry* 12 (2010): 2079–2079, https://doi.org/10.1039/c0gc00307g.

10. Y. Gu, N. Cui, Q. Yu, C. Li, and Q. Cui, "Study on the Influence of Channel Structure Properties in the Dehydration of Glycerol to Acrolein

Over H-Zeolite Catalysts," *Applied Catalysis A: General* 429–430 (2012): 9–16.

11. R. Almeida, M. F. Ribeiro, A. Fernandes, and J. P. Lourenço, "Gas-Phase Conversion of Glycerol to Allyl Alcohol Over Vanadium-Supported Zeolite Beta," *Catalysis Communications* 127 (2019): 20–24, https://doi.org/10.1016/j.catcom.2019.04.015.

12. G. Sánchez, B. Z. Dlugogorski, E. M. Kennedy, and M. Stockenhuber, "Zeolite-Supported Iron Catalysts for Allyl Alcohol Synthesis From Glycerol," *Applied Catalysis A: General* 509 (2016): 130–142, https://doi.org/10.1016/j.apcata.2015.09.039.

13. L. G. Possato, W. H. Cassinelli, T. Garetto, S. H. Pulcinelli, C. V. Santilli, and L. Martins, "One-Step Glycerol Oxidehydration to Acrylic Acid on Multifunctional Zeolite Catalysts," *Applied Catalysis A: General* 492 (2015): 243–251, https://doi.org/10.1016/j.apcata.2014.12.049.

14. S. Chaowamalee, A. Chotirattanachote, W. Khammee, C. Kalvibool, and C. Ngamcharussrivichai, "Sustainable Production of 1-Propanol via the Selective Hydrogenolysis of Glycerol Over a Tailored Iridium–Rhenium Oxide Catalyst Supported on HUSY Zeolite," *ChemCatChem* 17 (2025): e00885, https://doi.org/10.1002/cctc.202500885.

15. H. Mitta, P. K. Seelam, S. Ojala, R. L. Keiski, and P. Balla, "Tuning Y-Zeolite Based Catalyst With Copper for Enhanced Activity and Selectivity in Vapor Phase Hydrogenolysis of Glycerol to 1,2-Propanediol," *Applied Catalysis A: General* 550 (2018): 308–319, https://doi.org/10.1016/j.apcata.2017.10.019.

16. S. Chanklang, W. Mondach, P. Somchuea, et al., "Hydrogenolysis of Glycerol to 1,3-Propanediol Over H-ZSM-5-Supported Iridium and Rhenium Oxide Catalysts," *Catalysis Today* 397–399 (2022): 356–364, https://doi.org/10.1016/j.cattod.2021.08.014.

17. H. J. Cho, C. C. Chang, and W. Fan, "Base Free, One-Pot Synthesis of Lactic Acid From Glycerol Using a Bifunctional Pt/Sn-MFI Catalyst," *Green Chemistry* 16 (2014): 3428–3433, https://doi.org/10.1039/C4GC00723A.

18. B. Tang, X. Zuo, A. Li, et al., "Lewis Acidic Zeolite-Encapsulated Bimetallic Au–Pt Nanoparticles as Robust Catalysts for the Conversion of Glycerol to Methyl Lactate," *ACS Catalysis* 15 (2025): 16953–16967, https://doi.org/10.1021/acscatal.5c03831.

19. M. Tamura, W. Chaikittisilp, T. Yokoi, and T. Okubo, "Incorporation Process of Ti Species Into the Framework of MFI Type Zeolite," *Microporous and Mesoporous Materials* 112 (2008): 202–210, https://doi.org/10.1016/j.micromeso.2007.09.044.

20. T. Wu, S. Juan Li, G. Mei Yuan, et al., "Enhanced Selectivity of Propylene in Butylene Catalytic Cracking Over W-ZSM-5," *Fuel Processing Technology* 173 (2018): 143–152, https://doi.org/10.1016/j.fuproc.2018.01.022.

21. P. Pornsetmetakul, F. J. A. G. Coumans, R. C. J. van de Poll, et al., "Post-Synthesis Metal (Sn, Zr, Hf) Modification of BEA Zeolite: Combined Lewis and Brönsted Acidity for Cascade Catalysis," *Chinese Journal of Catalysis* 55 (2023): 200–215, https://doi.org/10.1016/S1872-2067(23)64539-5.

22. M. Boronat, P. Concepción, A. Corma, M. Renz, and S. Valencia, "Determination of the Catalytically Active Oxidation Lewis Acid Sites in Sn-Beta Zeolites, and Their Optimisation by the Combination of Theoretical and Experimental Studies," *Journal of Catalysis* 234 (2005): 111–118, https://doi.org/10.1016/j.jcat.2005.05.023.

23. P. Li, G. Liu, H. Wu, Y. Liu, J. G. Jiang, and P. Wu, "Postsynthesis and Selective Oxidation Properties of Nanosized Sn-Beta Zeolite," *Journal of Physical Chemistry C* 115 (2011): 3663–3670, https://doi.org/10.1021/jp1076966.

24. C. Hammond, S. Conrad, and I. Hermans, "Simple and Scalable Preparation of Highly Active Lewis Acidic Sn-$\beta$," *Angewandte Chemie International Edition* 51 (2012): 11736–11739, https://doi.org/10.1002/anie.201206193.

25. T. Lu, X. You, Y. Zong, Y. Xu, X. Yang, and L. Zhou, "Production of $\gamma$-Valerolactone From Ethyl Levulinate Over Hydrothermally Synthesized Sn-Beta Under Mild Conditions," *Fuel* 332 (2023): 126262–126262, https://doi.org/10.1016/j.fuel.2022.126262.

26. B. Tang, W. Dai, G. Wu, N. Guan, L. Li, and M. Hunger, "Improved Postsynthesis Strategy to Sn-Beta Zeolites as Lewis Acid Catalysts for the Ring-Opening Hydration of Epoxides," *ACS Catalysis* 4 (2014): 2801–2810, https://doi.org/10.1021/cs500891s.

27. J. Dijkmans, J. Demol, K. Houthoofd, S. Huang, Y. Pontikes, and B. Sels, "Post-Synthesis Sn$\beta$: An Exploration of Synthesis Parameters and Catalysis," *Journal of Catalysis* 330 (2015): 545–557, https://doi.org/10.1016/j.jcat.2015.06.023.

28. H. Zhang, Z. J. Quek, S. Jaenicke, and G. K. Chuah, "Hydrophobicity and co-Solvent Effects on Meerwein-Ponndorf-Verley Reduction/Dehydration Cascade Reactions Over Zr-Zeolite Catalysts," *Journal of Catalysis* 400 (2021): 50–61, https://doi.org/10.1016/j.jcat.2021.05.011.

29. C. García-Sancho, R. Moreno-Tost, J. Mérida-Robles, J. Santamaría-González, A. Jiménez-López, and P. Maireles-Torres, "Zirconium Doped Mesoporous Silica Catalysts for Dehydration of Glycerol to High Added-Value Products," *Applied Catalysis A: General* 433-434 (2012): 179–187, https://doi.org/10.1016/j.apcata.2012.05.015.

30. A. Kant, Y. He, A. Jawad, et al., "Hydrogenolysis of Glycerol Over Ni, Cu, Zn, and Zr Supported on H-Beta," *Chemical Engineering Journal* 317 (2017): 1–8.

31. S.-H. Chai, H.-P. Wang, Y. Liang, and B.-Q. Xu, "Sustainable Production of Acrolein: Investigation of Solid Acid–Base Catalysts for Gas-Phase Dehydration of Glycerol," *Green Chemistry* 9 (2007): 1130–1130.

32. A. Fernandes, M. F. Ribeiro, and J. P. Lourenço, "Conversion of Glycerol Over Vanadium Supported Beta Zeolite: Role of Acidity and Alkali Cations," *Microporous and Mesoporous Materials* 329 (2022): 111536, https://doi.org/10.1016/j.micromeso.2021.111536.

33. R. J. Chimentão, B. C. Miranda, D. Ruiz, et al., "Catalytic Performance of Zinc-Supported Copper and Nickel Catalysts in the Glycerol Hydrogenolysis," *Journal of Energy Chemistry* 42 (2020): 185–194, https://doi.org/10.1016/j.jechem.2019.07.003.

34. J. Wang, J. Wang, J. Xie, and Y. Zhou, "New Facile Way to Isomorphously Substituted Cr-$\beta$ Zeolite and Its Catalytic Performance," *Microporous and Mesoporous Materials* 171 (2013): 87–93, https://doi.org/10.1016/j.micromeso.2012.12.027.

35. J. El Haskouri, S. Cabrera, C. Guillem, et al., "Atrane Precursors in the One-Pot Surfactant-Assisted Synthesis of High Zirconium Content Porous Silicas," *Chemistry of Materials* 14 (2002): 5015–5022, https://doi.org/10.1021/cm020131u.

36. M. S. Morey, G. D. Stucky, S. Schwarz, and M. Fröba, "Isomorphic Substitution and Postsynthesis Incorporation of Zirconium Into MCM-48 Mesoporous Silica," *Journal of Physical Chemistry B* 103 (1999): 2037–2041, https://doi.org/10.1021/jp980844t.

37. H. Su, Z. Zong, W. Lou, et al., "An Efficient Zr-ZSM-5-st Solid Acid Catalyst for the Polyol Esterification Reaction," *Catalysts* 12 (2022): 901.

38. Y. Yang, D. Zhou, H. Zhang, et al., "In-Situ Construction and Catalytic Property of Highly Exposed Lewis Acidity on Hierarchical Zr-Zeolite Assisted by K+ Cation," *Microporous and Mesoporous Materials* 324 (2021): 110898–110898, https://doi.org/10.1016/j.micromeso.2021.110898.

39. R. Baran, Y. Millot, T. Onfroy, J. M. Krafft, and S. Dzwigaj, "Influence of the Nitric Acid Treatment on Al Removal, Framework Composition and Acidity of BEA Zeolite Investigated by XRD, FTIR and NMR," *Microporous and Mesoporous Materials* 163 (2012): 122–130, https://doi.org/10.1016/j.micromeso.2012.06.055.

40. Y. Hu, Q. He, and C. Xu, "Catalytic Conversion of Glycerol Into Hydrogen and Value-Added Chemicals: Recent Research Advances," *Catalysts* 11 (2021): 1455.

41. P. Salas, J. A. Wang, H. Armendariz, C. Angeles-Chavez, and L. F. Chen, "Effect of the Si/Zr Molar Ratio on the Synthesis of Zr-Based Mesoporous Molecular Sieves," *Materials Chemistry and Physics* 114 (2009): 139–144, https://doi.org/10.1016/j.matchemphys.2008.08.086.

42. J. Wang, S. Jaenicke, and G. K. Chuah, "Zirconium-Beta Zeolite as a Robust Catalyst for the Transformation of Levulinic Acid to γ-Valerolactone via Meerwein-Ponndorf-Verley Reduction," *RSC Advances* 4 (2014): 13481–13489.

43. J. Wang, K. Okumura, S. Jaenicke, and G. K. Chuah, "Post-Synthesized Zirconium-Containing Beta Zeolite in Meerwein–Ponndorf–Verley Reduction: Pros and Cons," *Applied Catalysis A: General* 493 (2015): 112–120, https://doi.org/10.1016/j.apcata.2015.01.001.

44. X. Liu, B. Yin, W. Zhang, et al., "Catalytic Transfer Hydrogenolysis of Glycerol Over Heterogeneous Catalysts: A Short Review on Mechanistic Studies," *Chemical Record* 21 (2021): 1792–1810, https://doi.org/10.1002/tcr.202100037.

45. A. Torres, D. Roy, B. Subramaniam, and R. V. Chaudhari, "Kinetic Modeling of Aqueous-Phase Glycerol Hydrogenolysis in a Batch Slurry Reactor," *Industrial & Engineering Chemistry Research* 49 (2010): 10826–10835, https://doi.org/10.1021/ie100553b.

46. A. V. H. Soares, G. Perez, and F. B. Passos, "Alumina Supported Bimetallic Pt–Fe Catalysts Applied to Glycerol Hydrogenolysis and Aqueous Phase Reforming," *Applied Catalysis B: Environmental* 185 (2016): 77–87, https://doi.org/10.1016/j.apcatb.2015.11.003.

47. T. Miyazawa, Y. Kusunoki, K. Kunimori, and K. Tomishige, "Glycerol Conversion in the Aqueous Solution Under Hydrogen Over Ru/$C^+$ an Ion-Exchange Resin and Its Reaction Mechanism," *Journal of Catalysis* 240 (2006): 213–221, https://doi.org/10.1016/j.jcat.2006.03.023.

48. S. K. Tanielyan, N. Marin, G. Alvez, et al., "An Efficient, Selective Process for the Conversion of Glycerol to Propylene Glycol Using Fixed Bed Raney Copper Catalysts," *Organic Process Research & Development* 18 (2014): 1419–1426, https://doi.org/10.1021/op400123f.

49. B. C. Miranda, R. J. Chimentão, J. B. O. Santos, et al., "Conversion of Glycerol Over 10%Ni/γ-$Al_2O_3$ catalyst," *Applied Catalysis B: Environmental* 147 (2014): 464–480.

50. E. P. Maris and R. J. Davis, "Hydrogenolysis of Glycerol Over Carbon-Supported Ru and Pt Catalysts," *Journal of Catalysis* 249 (2007): 328–337, https://doi.org/10.1016/j.jcat.2007.05.008.

51. S. Kandasamy, S. P. Samudrala, and S. Bhattacharya, "The Route Towards Sustainable Production of Ethylene Glycol From a Renewable Resource, Biodiesel Waste: A Review," *Catalysis Science & Technology* 9 (2019): 567–577, https://doi.org/10.1039/C8CY02035C.

52. N. Ueda, Y. Nakagawa, and K. Tomishige, "Conversion of Glycerol to Ethylene Glycol Over Pt-Modified Ni Catalyst," *Chemistry Letters* 39 (2010): 506–507, https://doi.org/10.1246/cl.2010.506.

53. A. Martin, U. Armbruster, I. Gandarias, and P. L. Arias, "Glycerol Hydrogenolysis Into Propanediols Using In Situ Generated Hydrogen—A Critical Review," *European Journal of Lipid Science and Technology* 115 (2013): 9–27, https://doi.org/10.1002/ejlt.201200207.

54. J. Feng and B. Xu, "Reaction Mechanisms for the Heterogeneous Hydrogenolysis of Biomass-Derived Glycerol to Propanediols," *Progress in Reaction Kinetics and Mechanism* 39 (2014): 1–15, https://doi.org/10.3184/97809059274714X13874723178485.

55. C. Montassier, D. Giraud, and J. Barbier, "Polyol Conversion by Liquid Phase Heterogeneous Catalysis Over Metals," *Studies in Surface Science and Catalysis* 41 (1988): 165–170.

56. M. G. Musolino, L. A. Scarpino, F. Mauriello, and R. Pietropaolo, "Selective Transfer Hydrogenolysis of Glycerol Promoted by Palladium Catalysts in Absence of Hydrogen," *Green Chemistry* 11 (2009): 1511–1513, https://doi.org/10.1039/b915745j.

57. E. Tsukuda, S. Sato, R. Takahashi, and T. Sodesawa, "Production of Acrolein From Glycerol Over Silica-Supported Heteropoly Acids," *Catalysis Communications* 8 (2007): 1349–1353, https://doi.org/10.1016/j.catcom.2006.12.006.

58. W. Suprun, M. Lutecki, T. Haber, and H. Papp, "Acidic Catalysts for the Dehydration of Glycerol: Activity and Deactivation," *Journal of Molecular Catalysis A: Chemical* 309 (2009): 71–78, https://doi.org/10.1016/j.molcata.2009.04.017.

59. A. Corma, G. W. Huber, L. Sauvanaud, and P. O'Connor, "Biomass to Chemicals: Catalytic Conversion of Glycerol/Water Mixtures Into Acrolein, Reaction Network," *Journal of Catalysis* 257 (2008): 163–171, https://doi.org/10.1016/j.jcat.2008.04.016.

60. T. Atchimarungsri, X. Gao, Q. Ma, et al., "Highly Efficient Conversion of Glycerol to Acetaldehyde Over $In_2O_3$/HZSM-5 Catalysts," *ACS Sustainable Chemistry & Engineering* 10 (2022): 11078–11087, https://doi.org/10.1021/acssuschemeng.2c00933.

61. A. E. Ferreira, M. L. Cerrada, E. Pérez, et al., "UHMWPE/SBA-15 Nanocomposites Synthesized by In Situ Polymerization," *Microporous and Mesoporous Materials* 232 (2016): 13–25, https://doi.org/10.1016/j.micromeso.2016.06.002.

## Supporting Information

Additional supporting information can be found online in the Supporting Information section.

**Supporting File**: cctc70771-sup-0001-SuppMat.docx.